# Full-Wave Analysis of Coplanar Waveguides by Variational Conformal Mapping Technique

CHIA-NAN CHANG, YU-CHING WONG, AND CHUN HSIUNG CHEN, SENIOR MEMBER, IEEE

*Abstract*—**A new full-wave analysis of coplanar waveguides is presented. A modification of Wen's mapping is combined with the variational formulation to facilitate a finite-element solution. This mapping function transforms the infinite original domain into a finite image domain and also overcomes the difficulty of field singularities near the conductor edges. In this study, numerical results for the frequency-dependent effective dielelectric constants and characteristic impedances of coplanar waveguides are presented. Particular attention is given to the electric field distributions over the air–dielectric interface of slots and the current distributions on the signal strip. Comparisons are also made between the computed results and available ones.**

## I. Introduction

COPLANAR waveguides (CPW's) have been the subject of extensive study [1]–[11] because they are easily adapted to the active or passive components in shunt or series configurations. Drilling of holes or slots through the substrate is not needed. Therefore, various applications of coplanar waveguide in microwave integrated circuits (MIC's) have been suggested, for instance, as detectors [1], balance mixers [3], and directional couplers [4]. In the design of these circuits it is important to calculate the propagation constant, the field pattern, and the characteristic impedance of the coplanar waveguide.

Since coplanar waveguides are inhomogeneous open structures with fields extending to infinity, many investigators have proposed the conformal mapping technique together with the quasi-static approximation [5]–[9]. Wen [5] initiated such an analysis in 1969 by using a mapping function in term of complete elliptic integrals and making the assumption that the dielectric substrate is thick enough to be considered infinite. By a modification of Wen's method, Davis *et al.* [6] later took the thickness of dielectric substrate into account. Hanna and Thebault [7] studied the asymmetric effect of slots by using a combined hyperbolic mapping function. Ghione and Naldi [8] investigated the parasitic effects in an actual realization of a coplanar waveguide, also using a suitable mapping function. Recently, Wong [9] combined the finite-element and conformal-mapping techniques to give a better understanding of the coplanar waveguide. All these works, however, were based on the quasi-static approximation and could not reveal the frequency-dependent behavior of the important parameters.

To date, full-wave analysis of the coplanar waveguiding structures was mainly carried out in the spectral domain [10], [11]. Fujiki and Kitazawa [10] studied the dispersive characteristics of coplanar waveguide modes by applying the Galerkin method to the simultaneous integral equations for the tangential magnetic fields over the slot. In their study, the waveguide is bounded by perpendicular conducting sidewalls and hence is a semiclosed structure. Knorr and Kucher [11] studied the frequency-dependent parameters of an unbound coplanar waveguide by applying the Galerkin method to the assumed tangential electric field over the slot.

In this paper, a rigorous full-wave method that involves combining the conformal mapping technique and variation reaction theory [12] is proposed. This method has proved to be successful in handling open dielectric waveguides [13] and microstrip lines [14]. In this work, the mapping function originally employed by Wen [5] is used to map the original infinite domain into a finite image domain and also to account for the singularity of fields near the conductor edges. Here, the finite thickness of the dielectric substrate is considered together with the assumptions of lossless guides and negligible metallization thickness. The current distributions on the center signal strip as well as the tangential electric fields over the slot along the air–dielectric interface are examined. The frequency-dependent effective dielectric constants and characteristic impedances are then calculated and compared with available data by other investigators [11].

## II. Method of Analysis

The open uniform coplanar waveguide under investigation is shown in Fig. 1, where a central metal strip of width $2a$ and two ground planes of separation $2b$ are placed on a substrate with relative permittivity $\epsilon_r$ and thickness $h$. The guided modes of this inhomogeneous structure are in general hybrid; therefore, both axial components $E_z$ and $H_z$ are required in the analysis. As far as

Manuscript received August 16, 1989; revised April 5, 1990. This work was supported by the National Science Council, Republic of China, under Grant NSC 79-0404-E002-39.

The authors are with the Department of Electrical Engineering, National Taiwan University, Taipei 10764, Taiwan, Republic of China.

IEEE Log Number 9036763.

0018-9480/90/0900-1339$01.00 ©1990 IEEE

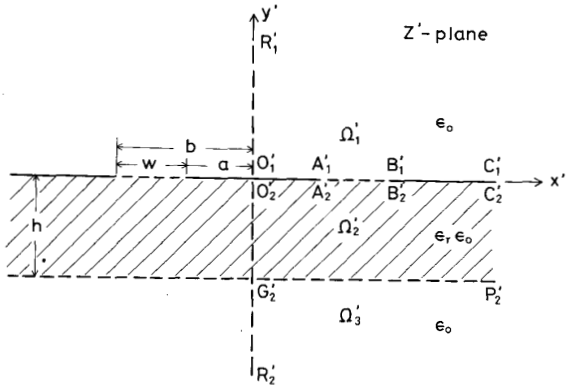


Fig. 1. Geometry of coplanar waveguide and definition of original domain $\Omega' = \Omega_1' + \Omega_2' + \Omega_3'$ ($x' \geq 0$) in $z'$ plane.

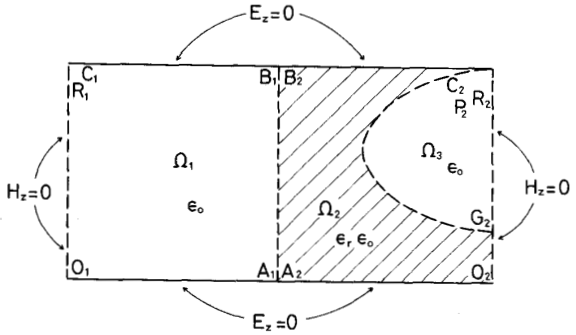


Fig. 2. Corresponding image domain $\Omega = \Omega_1 + \Omega_2 + \Omega_3$ in $z$ plane.

the dominant ($E_z$ even and $H_z$ odd) mode is concerned, it is sufficient to consider the right half structure with a magnetic wall on $x' = 0$.

By the variational conformal mapping technique, the coplanar waveguide in the original $z'$ plane (Fig. 1) may be analyzed in the finite image $z$ domain (Fig. 2) by using the $(E_z, H_z)$ formulation as follows [13], [14]:

$$\delta I = 0$$

$$I = \int\int_{\Omega} d\Omega \left(\frac{1}{\epsilon_r \mu_r - \epsilon_{\text{eff}}}\right) \begin{bmatrix} z \times \nabla_t E_z^a \\ \eta_0 \nabla_t H_z^a \end{bmatrix}^T \cdot \begin{bmatrix} \epsilon_r & -\sqrt{\epsilon_{\text{eff}}} \\ \sqrt{\epsilon_{\text{eff}}} & -\mu_r \end{bmatrix} \begin{bmatrix} z \times \nabla_t E_z \\ \eta_0 \nabla_t E_z \end{bmatrix} - k^2 \int\int_{\Omega} J d\Omega \begin{bmatrix} E_z^a \\ H_z^a \end{bmatrix}^T \begin{bmatrix} \epsilon_r & 0 \\ 0 & -\mu_r \end{bmatrix} \begin{bmatrix} E_z \\ H_z \end{bmatrix} \quad (1)$$

where $(E_z^a, H_z^a)$ and $(E_z, H_z)$ are the weighting and trial fields [14], respectively. Here, $J$ denotes the Jacobian of the mapping function, and the integration region $\Omega$ extends over the finite image domain (Fig. 2). The parameters $\epsilon_r$ and $\mu_r$ denote the relative permittivity and permeability of the substrate, while $\eta_0$ and $k$ are the intrinsic impedance and wavenumber of free space, respectively. The effective dielectric constant $\epsilon_{\text{eff}}$ is defined as

$$\epsilon_{\text{eff}} = (\beta / k)^2 \quad (2)$$

where $\beta$ denotes the propagation constant in the waveguide.

Using the double periodic property of the sine elliptic function [15], [16], it can be proved that the mapping function

$$z' = a\,\text{sn}(z, k) \quad (3)$$

maps the right half plane $x' \geq 0$ ($\Omega' = \Omega_1' + \Omega_2' + \Omega_3'$) in the original domain (Fig. 1) into a rectangular region of width $2K(k)$ and height $K(k')$ ($\Omega = \Omega_1 + \Omega_2 + \Omega_3$) in the image domain (Fig. 2). Here, $\text{sn}(z, k)$ is the sine elliptic function, $K(k)$ and $K(k')$ are the complete elliptic integrals of first kind and second kind [15], [16], $k = a/b$, and $k' = \sqrt{1 - k^2}$. The Jacobian of the function in (3) is

$$J = |dz'/dz|^2_{z=(x,y)} = a^2 \left|(1 - \text{sn}^2(z, k))(1 - k^2\,\text{sn}^2(z, k))\right|^2 \quad (4)$$

from which one may verify that $J \to r'$ near the strip edge, where $r'$ is the distance from the conductor edge in the original domain.

Once the longitudinal and transverse fields, $(E_z, H_z)$ and $(\vec{E}_t, \vec{H}_t)$, in the image domain are evaluated from (1), one can calculate the corresponding transverse fields $(\vec{E}_t', \vec{H}_t')$ in the original domain [14]:

$$\vec{E}_t' = \frac{|\vec{E}_t|}{\sqrt{J}} \left[\cos(\Psi_e + \theta)\,\hat{x} + \sin(\Psi_e + \theta)\,\hat{y}\right] \quad (5)$$

$$\vec{H}_t' = \frac{|\vec{H}_t|}{\sqrt{J}} \left[\cos(\Psi_h + \theta)\,\hat{x} + \sin(\Psi_h + \theta)\,\hat{y}\right]. \quad (6)$$

Here $\theta$ denotes the argument of the first derivative of the mapping function, and $\Psi_e$ and $\Psi_h$ are the angles between the two components of $\vec{E}_t$ and $\vec{H}_t$, respectively. From edge condition analysis, the transverse fields $(\vec{E}_t', \vec{H}_t')$ near the strip edges are proportional to $r'^{-1/2}$ [17]. However, the $\sqrt{J}$ factor in (5) and (6) renders the fields $(\vec{E}_t, \vec{H}_t)$ smooth over the image domain.

To solve (1) by the finite-element method [18], one first discretizes the image domain $\Omega$ into a finite number of isoparametric triangular elements, each with six nodes as shown in Fig. 3(a). The six second-order shape functions $N_1$ to $N_6$ are defined by

$$N_1 = L_1(2L_1 - 1) \qquad N_2 = L_2(2L_2 - 1)$$
$$N_3 = L_3(2L_3 - 1) \qquad N_4 = 4L_1L_2$$
$$N_5 = 4L_2L_3 \qquad N_6 = 4L_3L_1 \quad (7)$$

where $L_1$, $L_2$, and $L_3$ are the local coordinates of any point in an element. The relation between the local area coordinates and the global coordinates $(x, y)$ of a point in an element is given by

$$\begin{bmatrix} x \\ y \\ 1 \end{bmatrix} = \begin{bmatrix} x_1 & x_2 & x_3 \\ y_1 & y_2 & y_3 \\ 1 & 1 & 1 \end{bmatrix} \begin{bmatrix} L_1 \\ L_2 \\ L_3 \end{bmatrix} \quad (8)$$

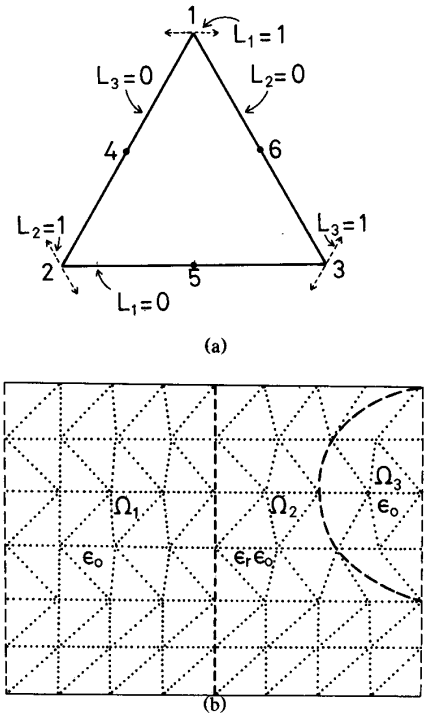


Fig. 3. (a) Nodes and area coordinates for second-order triangular element. (b) Typical subdivision in image domain.

where $(x_i, y_i)$, $i = 1,2,3$, are the global Cartesian coordinates of the $i$th vertex of the triangle (Fig. 3(a)). In each element, the field $\phi$ (which denotes $E_z$ or $H_z$) at any point is interpolated as

$$\phi = \sum_{i=1}^{6} \phi_i N_i \tag{9}$$

where $\phi_i$ denotes the nodal unknown. The integral over each element is calculated by the Gaussian–Hammer quadrature [18]. By assembling the calculated results for each element, one finally obtains a matrix equation by the Rayleigh–Ritz procedure, viz.

$$[A][\phi] = k^2[B][\phi] \tag{10}$$

where $[\phi]$ is the column vector corresponding to all nodal unknowns, and $[A]$ and $[B]$ are known sparse matrices. Although $[A]$ is not positive definite, (10) can still be effectively solved by the determinant search together with the inverse iteration method [19].

## III. Numerical Results and Discussion

Based on the procedures described in Section II, a computer software package has been developed on the VAX-11/780 computer which also includes an automatic mesh generation of second-order triangular elements in the image domain. In Fig. 3(b), a typical mesh division is shown. By investigating the effective dielectric constants of several typical coplanar lines ($\epsilon_r = 13$, $h = 1.5$ mm, $a/b = 0.2 \sim 0.6$) it is found that a mesh division of $16 \times 16 = 256$ elements is usually enough to give results with four-digit accuracy. Since the matrices in (10) are sparse, a skyline storage scheme [19] for matrix elements is used to save computer memory. To improve the convergence rate of the iteration in the eigensystem, the Cholesky decomposition [20] is employed for the system in (10).

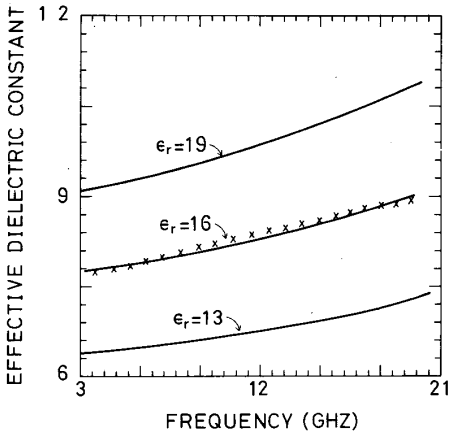


Fig. 4. Effective dielectric constant versus frequency with $\epsilon_r$ as parameters ($a = 0.5$ mm, $b = 0.9$ mm, $h = 1$ mm). Results of Knorr and Kuchler [11] $\times\times\times\times$ are given for comparison.

Numerical results for the coplanar waveguide, including the effective dielectric constants, the field distributions over the slot in the air–dielectric interface, the current distributions on the signal strip, and the characteristic impedances, will next be presented and discussed.

### A. Effective Dielectric Constant

Fig. 4 shows the frequency-dependent effective dielectric constants for different materials. Also shown for comparison in Fig. 4 are the results of Knorr and Kuchler [11] for $\epsilon_r = 16$. Agreement between the two is observed, with a pointwise difference of at most 2%.

In Fig. 5, the frequency dependence of the effective dielectric constant is plotted with $h/b$ as a parameter. Small values of $h/b$ correspond to wider widths of both the signal strip and the slot. The arrows at the left of each curve indicate the corresponding quasi-static values calculated by Wong [9] and by Kitazawa and Hayashi [21]. Excellent agreement at the low-frequency limit is evident.

### B. Field Distributions

The normalized tangential field distributions $E_x/E_{x_{\min}}$ and $E_z/E_{z_{\max}}$ over the slot are presented in Fig. 6. The ratio $E_z/E_x$ at any point over the slot is smaller than 1/100, which makes the zero longitudinal field assumption in the spectral-domain analysis acceptable. As expected, the normalized transverse field $E_x/E_{x_{\min}}$ exhibits the edge singularity near the conductor edges. The frequency independence and symmetric distribution of this transverse field are the essential assumptions of the spectral-domain method [11], and these are again supported by this study.

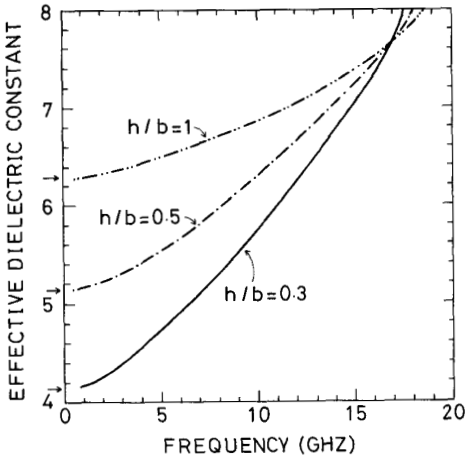


Fig. 5. Effective dielectric constant versus frequency with $h/b$ as parameters ($h = 1.5$ mm, $\epsilon_r = 13$, $a/b = 0.4$).

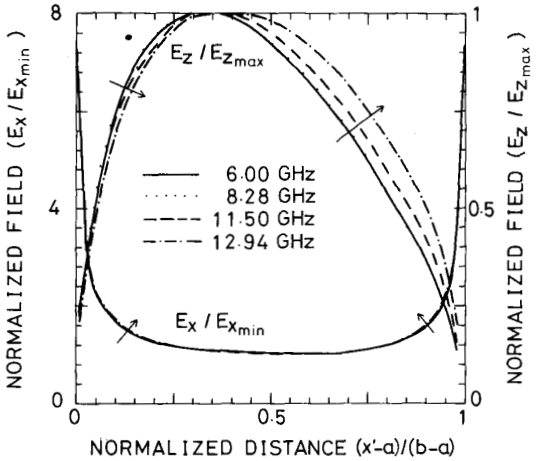


Fig. 6. Normalized field distributions over slot with frequencies as parameters ($a = 1.2$ mm, $b = 2.4$ mm, $h = 1.2$ mm, $\epsilon_r = 13$).

### C. Current Distributions

Shown in Fig. 7 are the normalized longitudinal and transverse current distributions at different frequencies. Again, the longitudinal current exhibits an edge singularity at points near the strip edge. The arrows in Fig. 7 indicate the tendency of the normalized currents as the frequency is increased. This tendency is contrary to that of microstrip lines [14] owing to the different configuration of ground planes in the two structures.

It is noted that the current distributions for different dielectric constants of the substrate are hardly distinguishable. This behavior is the same as in microstrip lines [14].

### D. Characteristic Impedance

Three definitions for characteristic impedance are discussed and compared. They can be evaluated both in the original domain and in the image domain:

$$Z_{oi} = \frac{2P}{|I_{zt}|^2} \tag{11a}$$

$$Z_{vi} = \frac{|V_s|}{|I_{zt}|} \tag{11b}$$

$$Z_{ov} = \frac{|V_s|^2}{2P}. \tag{11c}$$

Here $P$ and $I_{zt}$ denote the power along the guide and the total longitudinal current on the strip [14], while $V_s$ is the voltage defined along the air–dielectric interface of the slot.

Since the integration region is finite and the fields are nonsingular in the image domain, we calculate all quantities in this domain. Fig. 8 shows the frequency dependence of impedances for different cases. The increase in strip width causes an increase in capacitance of the coplanar structure in the quasi-static approximation. Thus the characteristic impedances for a given frequency decrease as the strip width is increased, as indicated in Fig. 8. The

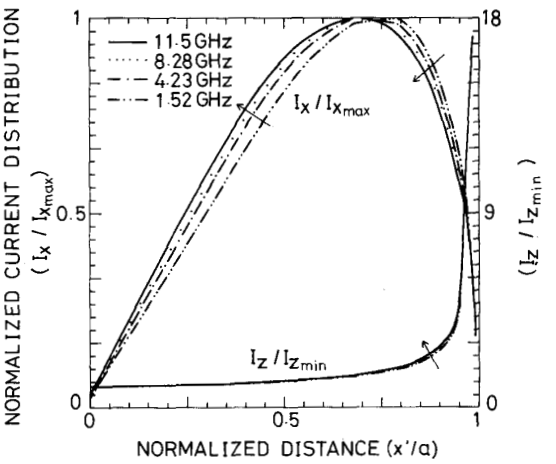


Fig. 7. Normalized current distributions on signal strip with frequencies as parameters ($a = 1.2$ mm, $b = 2.4$ mm, $h = 1.2$ mm, $\epsilon_r = 13$).

corresponding quasi-static values [9], [21] are indicated by the arrows. It is noted that the impedance $Z_{oi}$ based on current and power tends to the quasi-static value whereas $Z_{ov}$ and $Z_{vi}$ do not. Note also that the geometric mean of the $Z_{oi}$ and $Z_{ov}$ curves gives $Z_{vi}$ as defined by (11b).

In Fig. 9, the frequency dependences of characteristic impedances for different materials are plotted. The crosses in this figure are the results for $Z_{ov}$ for $\epsilon_r = 16$ in the spectral-domain method [11]. Agreement between the two is observed, with a pointwise deviation of at most 3%.

## IV. Conclusions

A new full-wave analysis of coplanar waveguides has been presented. By using a modification of Wen's mapping, the difficulties due to the finite domain and field singularities near the conductor edges have been properly treated. Numerical results for effective dielectric constants, field distributions, current distributions, and characteristic impedances have been computed and compared

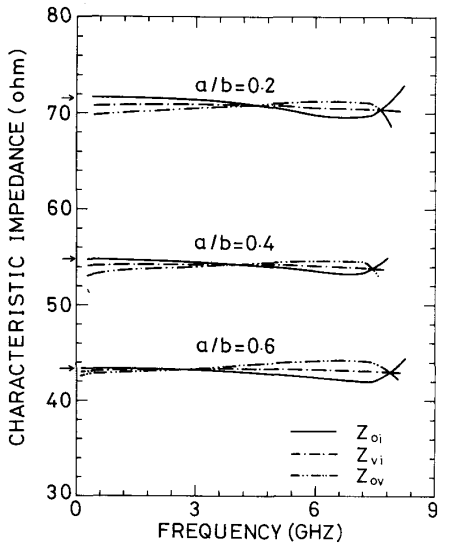


Fig. 8. Characteristic impedances versus frequency with $a/b$ as parameters ($b = 1.5$ mm, $h = 1.5$ mm, $\epsilon_r = 13$).

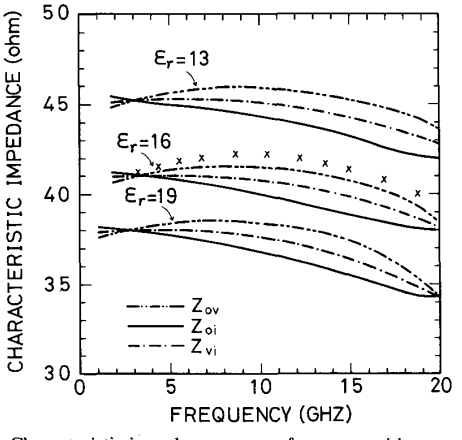


Fig. 9. Characteristic impedances versus frequency with $\epsilon_r$ as parameters ($a = 0.5$ mm, $b = 0.9$ mm, $h = 1$ mm). Results of Knorr and Kuchler [11] are denoted by $\times\times\times\times\times$.

with available data, and good agreement has been obtained.

By choosing suitable mapping functions, certain other waveguide problems can also be solved efficiently. Related work, such as the study of multilayer coplanar lines, is in progress and will be reported in the future.

## Acknowledgment

The authors wish to express their deep appreciation to Dr. R. B. Wu for valuable discussions.

## References

[1] M. Houdart, "Coupled lines: Applications to broadband microwave integrated circuits," in *Proc. 6th European Microwave Conf.* (Rome), 1976, pp. 49–53.

[2] K. C. Gupta, R. Garg, and I. J. Bahl, *Microstrip Lines and Slotlines*. Norwood MA: Artech House, 1979.

[3] E. L. Kollberg, *Microwave and Millimeter-Wave Mixers*. New York: IEEE Press, 1984.

[4] C. P. Wen, "Coplanar-waveguide directional couplers," *IEEE Trans. Microwave Theory Tech.*, vol. MTT-18, pp. 318–322, Apr. 1970.

[5] C. P. Wen, "Coplanar waveguide: A surface strip transmission line suitable for nonreciprocal gyromagnetic device applications," *IEEE Trans. Microwave Theory Tech.*, vol. MTT-17, pp. 1087–1090, Dec. 1969.

[6] M. E. Davis, E. W. Williams, and A. C. Celestini, "Finite-boundary corrections to the coplanar waveguide analysis," *IEEE Trans. Microwave Theory Tech.*, vol. MTT-21, pp. 594–596, Sept. 1973.

[7] V. Fouad Hanna and D. Thebault, "Analysis of asymmetrical coplanar waveguides," *Int. J. Electron.*, vol. 50, no. 3, pp. 221–224, Mar. 1981.

[8] G. Ghione and C. U. Naldi, "Coplanar waveguides for MMIC applications: Effect of upper shielding, conductor backing, finite-extent ground planes, and line-to-line coupling," *IEEE Trans. Microwave Theory Tech.*, vol. MTT-35, pp. 260–267, Mar. 1987.

[9] Y. C. Wong, "Quasi-static analysis of coplanar waveguides," master's thesis, Graduate Institute of Electrical Engineering, National Taiwan University, June 1989.

[10] Y. Fujiki and T. Kitazawa, "Higher-order modes in coplanar-type transmission lines," *Electron. and Commun.* Japan, vol. 58-B, pp. 74–80, 1975.

[11] J. B. Knorr and K. D. Kuchler, "Analysis of coupled slots and coplanar strips on dielectric substrate," *IEEE Trans. Microwave Theory Tech.*, vol. MTT-23, pp. 541–548, July 1975.

[12] R. B. Wu and C. H. Chen, "On the variational reaction theory for dielectric waveguides," *IEEE Trans. Microwave Theory Tech.*, vol. MTT-33, pp. 477–483, June 1985.

[13] R. B. Wu and C. H. Chen, "A variational analysis of dielectric waveguides by the conformal mapping techniques," *IEEE Trans. Microwave Theory Tech.*, vol. MTT-33, pp. 681–685, Aug. 1985.

[14] C. Shih, R. B. Wu, S. K. Jeng, and C. H. Chen, "A full-wave analysis of microstrip lines by variational conformal mapping technique," *IEEE Trans. Microwave Theory Tech.*, vol. 36, pp. 576–581, Mar. 1988.

[15] I. S. Gradshteyn and I. M. Ryzhik, *Table of Integrals, Series, and Products*. New York: Academic Press, 1965.

[16] F. Mathews and R. L. Walker, *Mathematical Methods of Physics*. New York: W. A. Benjamin, 1970.

[17] R. Mittra and S. W. Lee, *Analytical Techniques in the Theory of Guided Waves*. New York: Macmillan, 1971.

[18] O. C. Zienkiewicz, *The Finite Element Method*. New York: McGraw-Hill, 1977.

[19] K. J. Bathe and E. L. Wilson, *Numerical Methods in Finite Element Analysis*. Englewood Cliffs, NJ: Prentice-Hall, 1976.

[20] O. Axelsson and V. A. Barker, *Finite Element Solution of Boundary Value Problem—Theory and Computation*. New York: Academic Press, 1984.

[21] T. Kitazawa and Y. Hayashi, "Coupled slots on an anisotropic sapphire substrate," *IEEE Trans. Microwave Theory Tech.*, vol. MTT-29, pp. 1035–1040, Oct. 1981.

**Chia-Nan Chang** was born in Taipei, Taiwan, Republic of China, on September 4, 1943. He received the B.S. degree from National Taiwan Normal University, Taipei, Taiwan, in 1965 and the M.S. degree from National Taiwan University, Taipei, Taiwan, in 1969. Since 1986, he has been working toward the Ph.D. degree in electrical engineering at National Taiwan University.

In 1980, he joined the faculty of the Department of Electronic Engineering, National Tai-

wan Institute of Technology, Taipei, Taiwan, where he is now an instructor. He is currently engaged in the numerical analysis of coplanar waveguiding structures.

✠

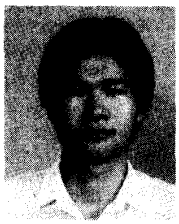

**Yu-Ching Wong** was born in Taipei, Taiwan, Republic of China, on September 30, 1964. He received the B.S.E.E. degree from Tamkang University, Taipei, Taiwan, in 1987 and the M.S.E.E. degree from the Institute of Electrical Engineering, National Taiwan University, Taipei, Taiwan, in 1989.

In July 1989 he joined the Chung-Shan Institute of Science and Technology, Taur-Yuan, Taiwan, where he is a research assistant. His interests include numerical methods for dielectric waveguides and the electrical circuits of synthesizers.

**Chun Hsiung Chen** (SM'88) was born in Taipei, Taiwan, Republic of China, on March 7, 1937. He received the B.S.E.E. degree from National Taiwan University, Taipei, Taiwan, in 1960, the M.S.E.E. degree from National Chiao Tung University, Hsinchu, Taiwan, in 1962, and the Ph.D. degree in electrical engineering from National Taiwan University in 1972.

In 1963, he joined the faculty of the Department of Electrical Engineering, National Taiwan University, where he is now a Professor. From August 1982 to July 1985 he was Chairman of the department. In 1974 he was a Visiting Researcher for one year in the Department of Electrical Engineering and Computer Sciences, University of California, Berkeley. From August 1986 to July 1987, he was a Visting Professor in the Department of Electrical Engineering, University of Houston, Texas. During June and July of 1989, he was a visitor in the Microwave Department, Technical University of Munich, West Germany. His areas of interest include antenna and waveguide analysis, propagation and scattering of waves, and numerical techniques in electromagnetics.